

Analytical solution of the unsteady Pennes equation for burn depth determination from dynamic infrared thermographs

R. Romero-Méndez¹, Dirk F. DeLange¹, Mihir Sen² and F.J. González³

¹*Facultad de Ingeniería, Universidad Autónoma de San Luis Potosí, San Luis Potosí, SLP, Mexico,* ²*Department of Aerospace and Mechanical Engineering, University of Notre Dame, Notre Dame, IN 46556, U.S.A.,* ³*Instituto de Investigación en Comunicación Óptica, Universidad Autónoma de San Luis Potosí, San Luis Potosí, SLP, Mexico*

September 6, 2009

Abstract

The paper analyzes the time-dependent thermal response of a burn that is suddenly subjected to a constant heat flux for the purpose of determining the depth of burned skin using dynamic thermography. The transient problem is modeled by the time-dependent Pennes bioheat equation for a superficial burned layer below which there is another layer of healthy tissue. The governing equations are simplified as one dimensional using a small burn-depth approximation. The initial condition used in the problem is the thermal equilibrium state previous to the imposition of a constant heat flux on the surface. An infinite series solution is found for the resulting equations. The analytical results were confirmed by comparison with a numerical solution. The validity of the one-dimensional approximation was evaluated by comparing with an axisymmetric numerical solution. The parametric dependence of the temperature response is analyzed. Measurement of the dynamic response of the skin surface temperature is found to be a valid way of simultaneously determining the properties of burned and unburned skin and the depth of burn.

1 Introduction

Temperature is commonly used as an indication and as a means of monitoring the progression of sickness [1]. The temperature distribution of skin has been used for diagnosis [2, 3], for follow-up treatments [4], and for the study of the physiological functions of healthy individuals [5]. In recent years the sensitivity of infrared sensors has improved considerably and is now close to 0.025°C, so that it is now possible to measure small changes in surface temperature [6]. The development of focal plane technologies has enabled the acquisition of high-quality images for computational processing. The emissivity of human skin has an

almost constant value of 0.97 ± 0.02 between wavelengths of $2 \mu\text{m}$ and $14 \mu\text{m}$ [7], behaving almost as a black body, and making it an ideal material for surface temperature measurements with an infrared camera [8–10]. The camera can also be used to take a sequence of thermographs at a suitable time interval, every 15 s say, to provide a dynamic picture of the temperature field.

A significant problem in burn therapy is the correct evaluation of skin burn depth which can have repercussions on the appropriate choice of treatment [11]. The current approach is to conservatively treat shallow wounds, which heal spontaneously within three weeks of the trauma, and to surgically intervene in deeper wounds which fail to heal during this period. However, the clinical assessment of burn-wound depth is mainly based on visual inspection. The traditional approach distinguishes the following grades of burn wound: I (superficial), IIa (superficial dermal), IIb (deep dermal), and III (full thickness of the skin). In clinical practice, even an inexperienced physician has no difficulty in classifying first- and third-degree burns correctly. However, differentiation between the IIa and IIb wounds is problematic even for the most experienced practitioners [12, 13]. Histopathological assessment is considered to be the reference method to determine skin burn depth, but even this procedure lacks commonly accepted quantitative criteria and, being invasive and local, is not frequently used in clinical practice [12]. In previous investigations related to the treatment of burns, good correlation has been shown between the difference in temperatures between burned and healthy skin and the depth of the burn. Zhu and Xin [14] determined that the correlation was better if the temperature difference was between a burned area and another symmetrical area of the body, but this measurement may not always be possible.

Infrared thermography of the skin has been used as a non-invasive method to determine burn depth by obtaining the temperature difference between the burned skin area and an unaffected reference skin area [12, 15]. The objective of the present work is to develop a *transient* methodology that will take a series of infrared thermographs of a burned area

at different instants of time in response to an external input, determine the time-dependent temperature response of the skin surface [16], and from that determine burn depth. Transient skin temperature has previously been suggested for this purpose [17], but the theoretical model was too simplistic to provide an accurate relationship between the measurements and the burn depth.

Theoretical modeling of burned skin has long been used to predict skin burn injury [18, 19], but can now also help develop a procedure to obtain burn depth from infrared thermographs. Romero-Méndez et al. [20], in a previous paper, proposed a steady-state technique for determination of the burn depth. They used a bioheat transfer model for skin, and solved it analytically to obtain an inverse procedure to determine burn depth from thermographs. However, it was assumed that the thermophysical properties of the burned and unburned skin were known, which is not commonly the case. Additional information is needed to simultaneously determine the skin properties also from the thermographs. This may be provided by the transient response of burned skin to a step input in external heat input, instead of just the steady state data. In active dynamic infrared thermal imaging [12], external or internal excitations are applied to an object to force time-dependent heat flows, producing spatial and surface temperature distributions which can give information on the thermal properties of the object. Cold stress, pharmacological excitation, or even electrical stimulation have been used for dynamic infrared imaging.

In the present work, the transient response of a 1D bioheat model of the skin subject to a step in external heating is determined. The analytical solution is verified with a numerical solution. The 1D approximation is evaluated using an axisymmetric numerical solution. The parametric dependence of the skin surface temperature is studied using the results produced by the analytical solution.

2 Governing equations

2.1 Mathematical model

The mathematical model for bioheat transfer used here is based on the Pennes equation [21]. This was derived for the situation where blood vessels cross a region. Some of the assumptions of the model are that the material is homogeneous and has isotropic thermal properties, the blood vessels are isotropic, and that the blood flow enters at arterial temperature but reaches the tissue temperature before leaving the arterial system. This model represents heat transfer in living tissue, and considers metabolic heat generation and convective heat transfer due to the perfusion of blood. It is important to mention that there are alternative models for bioheat transfer [22–24], such as the continuum model of Chen and Holmes [25], that of Weinbaum et al. [26] which considers the existence of large and small blood vessels, and other models that look at the tissue as a porous medium [27]. Procedures similar to the one described here can be adopted for these other models.

The unsteady Pennes equation for healthy tissue is

$$k\nabla^2 T + W_b C_b (T_a - T) + Q^* = \rho C \frac{\partial T}{\partial t}, \quad (1)$$

where $T(x, y, z, t)$ is the tissue temperature, k , ρ and C are the tissue thermal conductivity, density and specific heat, respectively, W_b is the blood perfusion rate, C_b is the blood specific heat, T_a is the arterial temperature, and Q^* is the tissue metabolic heat generation rate. x and y are the coordinates parallel to the surface of the skin, z is positive measured into the skin, and t is time.

2.2 Problem description

The skin is exposed to convective heat transfer to the surroundings, which is first at equilibrium with the generation of heat due to metabolism and perfusion. At $t = 0$ an external heat flux of constant value q^* is suddenly applied. The transient response of the temperature

distribution is to be determined as a function of system parameters. The purpose of this work is to find all these parameters including burn depth from dynamic surface temperature measurements. The surface temperature of the skin is $T_s(x, y, t) = T(x, y, 0, t)$.

Consider a three-dimensional region formed of two layers as shown in Figure 1. Layer 1 is a shallow, superficial burned region from $z = 0$ to $z = H(x, y)$, and layer 2 is a deep substrate of healthy tissue from $z = H(x, y)$ to $z = H_N$, where H_N is sufficiently deep. We assume that burned tissue is dead, blood perfusion and metabolic heat generation do not occur in such condition. From Eq. (1), the general, time-dependent governing equations are

$$k_1 \left(\frac{\partial^2 T_1}{\partial x^2} + \frac{\partial^2 T_1}{\partial y^2} + \frac{\partial^2 T_1}{\partial z^2} \right) = \rho_1 C_1 \frac{\partial T_1}{\partial t} \quad \text{for layer 1,} \quad (2a)$$

$$k_2 \left(\frac{\partial^2 T_2}{\partial x^2} + \frac{\partial^2 T_2}{\partial y^2} + \frac{\partial^2 T_2}{\partial z^2} \right) + W_b C_b (T_a - T_2) + Q^* = \rho_2 C_2 \frac{\partial T_2}{\partial t} \quad \text{for layer 2,} \quad (2b)$$

where the subscripts 1 and 2 refer to the two layers. The boundary conditions with an external irradiative flux q^* at $z = 0$ are

$$k_1 \frac{\partial T_1}{\partial z} = h(T_1 - T_\infty) + q^* \quad \text{at } z = 0, \quad (3a)$$

$$k_1 \frac{\partial T_1}{\partial z} = k_2 \frac{\partial T_2}{\partial z} \quad \text{at } z = H, \quad (3b)$$

$$T_1 = T_2 \quad \text{at } z = H, \quad (3c)$$

$$\frac{\partial T_2}{\partial z} = 0 \quad \text{at } z = H_N, \quad (3d)$$

and zero heat flux at all other boundaries, if any. h is the convective heat transfer coefficient at the surface, and T_∞ is the ambient temperature. Eq. (3a) is the heat balance at the surface and includes convective heat transfer as well as the irradiation; Eq. (3b) is the heat balance at the interface between layers 1 and 2; Eq. (3c) is the continuity of temperature at the interface; and Eq. (3d) represents zero heat flux far below the interface.

2.3 Nondimensionalization

We can scale the coordinates parallel and normal to the surface using the characteristic size R_c , and the characteristic depth H_c (the maximum value of $H(x, y)$, for example), of the burned region, respectively. The nondimensional variables are

$$\xi = \frac{x}{R_c}, \quad \eta = \frac{y}{R_c}, \quad \zeta = \frac{z}{H_c}, \quad \tau = \frac{\alpha_1}{H_c^2} t,$$

$$\theta_{1,2}(\xi, \eta, \zeta, \tau) = \frac{T_{1,2} - T_a}{T_\infty - T_a}, \quad \varphi(\xi, \eta) = \frac{H}{H_c},$$

where the thermal diffusivities are $\alpha_{1,2} = k_{1,2}/\rho_{1,2}C_{1,2}$. φ defines the nondimensional depth of the burned region. In general, T_a can be larger or smaller than T_∞ .

The governing equations (2) and boundary conditions (3) become

$$\begin{aligned} \epsilon \frac{\partial^2 \theta_1}{\partial \xi^2} + \epsilon \frac{\partial^2 \theta_1}{\partial \eta^2} + \frac{\partial^2 \theta_1}{\partial \zeta^2} &= \frac{\partial \theta_1}{\partial \tau} && \text{for } 0 \leq \zeta < \varphi, \\ \epsilon \frac{\partial^2 \theta_2}{\partial \xi^2} + \epsilon \frac{\partial^2 \theta_2}{\partial \eta^2} + \frac{\partial^2 \theta_2}{\partial \zeta^2} - m^2 \theta_2 - Q &= \frac{1}{\mu} \frac{\partial \theta_2}{\partial \tau} && \text{for } \varphi \leq \zeta < N\varphi, \\ \frac{\partial \theta_1}{\partial \zeta} &= \text{Bi} (\theta_1 - 1) + q && \text{at } \zeta = 0, \\ \frac{\partial \theta_1}{\partial \zeta} &= \kappa \frac{\partial \theta_2}{\partial \zeta} && \text{at } \zeta = \varphi, \\ \theta_1 &= \theta_2 && \text{at } \zeta = \varphi, \\ \frac{\partial \theta_2}{\partial \zeta} &= 0 && \text{at } \zeta = N\varphi, \end{aligned}$$

with zero heat flux at all other boundaries, if any. The nondimensional parameters are

$$m^2 = \frac{W_b C_b H_c^2}{k_2}, \quad \mu = \frac{\alpha_2}{\alpha_1}, \quad \text{Bi} = \frac{h H_c}{k_1}, \quad \epsilon = \frac{H_c^2}{R_c^2}$$

$$q = \frac{H_c q^*}{k_1 (T_\infty - T_a)}, \quad \kappa = \frac{k_2}{k_1}, \quad Q = \frac{Q^* H_c^2}{k_2 (T_a - T_\infty)}, \quad N = \frac{H_N}{H_c}.$$

where κ is the thermal conductivity ratio and μ is the thermal diffusivity ratio.

2.4 Small depth one-dimensional approximation

The equations are simplified if we assume $\epsilon \ll 1$. This is justified since in most cases burns are much more superficially extended than they are deep, so that the characteristic size is

much larger than the burn thickness. For instance, here we have used reasonable values of R_c and H_c which gives $\epsilon = 0.01$. The equations become one-dimensional for each point (ξ, η) on the surface of the skin. Essentially, since temperature gradients are small parallel to the surface, conduction in those directions is negligible compared to that in the normal direction. We can also assume $\varphi = 1$ locally as the problem is then one of a 1D burn with thickness $H = H_c$. The resulting equations are

$$\frac{\partial^2 \theta_1}{\partial \zeta^2} = \frac{\partial \theta_1}{\partial \tau} \quad \text{for } 0 \leq \zeta < 1, \quad (4a)$$

$$\frac{\partial^2 \theta_2}{\partial \zeta^2} - m^2 \theta_2 - Q = \frac{1}{\mu} \frac{\partial \theta_2}{\partial \tau} \quad \text{for } 1 \leq \zeta < N, \quad (4b)$$

$$\frac{\partial \theta_1}{\partial \zeta} = \text{Bi} (\theta_1 - 1) + q \quad \text{at } \zeta = 0, \quad (4c)$$

$$\frac{\partial \theta_1}{\partial \zeta} = \kappa \frac{\partial \theta_2}{\partial \zeta} \quad \text{at } \zeta = 1, \quad (4d)$$

$$\theta_1 = \theta_2 \quad \text{at } \zeta = 1, \quad (4e)$$

$$\frac{\partial \theta_2}{\partial \zeta} = 0 \quad \text{at } \zeta = N. \quad (4f)$$

3 Steady-state problems

There are two steady states of interest in the problem. The one with $q = 0$ in Eq. (4c) will be used as the initial condition for the transient problem at $t = 0$. The final condition at $t \rightarrow \infty$ with a constant, nonzero q will be needed in the transient solution.

The solution of Eqs. (4) with $\partial/\partial\tau = 0$ is

$$\theta_1^q(\zeta) = A_1^q \zeta + A_2^q, \quad (5a)$$

$$\theta_2^q(\zeta) = A_3^q \cosh m\zeta + A_4^q \sinh m\zeta - \frac{Q}{m^2}. \quad (5b)$$

The constants are

$$\begin{aligned}
A_1^q &= \frac{1}{B} \left[-m\kappa(\text{Bi} + \text{Bi} \frac{Q}{m^2} - q) (\sinh m - \tanh mN \cosh m) \right], \\
A_2^q &= \frac{1}{B} \left[m\kappa(\text{Bi} - \frac{Q}{m^2} - q) (\sinh m - \tanh mN \cosh m) \right. \\
&\quad \left. - (\text{Bi} - q) (\cosh m - \tanh mN \sinh m) \right], \\
A_3^q &= -\frac{1}{B} \left(\text{Bi} + \text{Bi} \frac{Q}{m^2} - q \right), \\
A_4^q &= \frac{1}{B} \left(\text{Bi} + \text{Bi} \frac{Q}{m^2} - q \right) \tanh mN,
\end{aligned}$$

where

$$B = m\kappa(\text{Bi} + 1) (\sinh m - \tanh mN \cosh m) - \text{Bi} (\cosh m - \tanh mN \sinh m). \quad (6)$$

Solutions θ_1^0 and θ_2^0 with $q = 0$ are a special case of Eq. (5).

4 Transient problem

The time-dependent solution of Eqs. (4) is split into two parts

$$\theta_{1,2}(\zeta, \tau) = \theta_{1,2}^q(\zeta) + \Psi_{1,2}(\zeta, \tau) \quad (7)$$

where $\theta_{1,2}^q$ from Eq. (5) are the $t \rightarrow \infty$ steady-state solutions. This is done so that the functions $\Psi_{1,2} \rightarrow 0$ as $t \rightarrow \infty$ and can be represented by vanishing exponentials. From Eqs. (4), $\Psi_{1,2}$ satisfies

$$\frac{\partial^2 \Psi_1}{\partial \zeta^2} = \frac{\partial \Psi_1}{\partial \tau} \quad \text{for } 0 \leq \zeta < 1, \quad (8a)$$

$$\frac{\partial^2 \Psi_2}{\partial \zeta^2} - m^2 \Psi_2 = \frac{1}{\mu} \frac{\partial \Psi_2}{\partial \tau} \quad \text{for } 1 \leq \zeta < N, \quad (8b)$$

subject to boundary conditions

$$\frac{\partial \Psi_1}{\partial \zeta} = \text{Bi} \Psi_1 \quad \text{at } \zeta = 0, \quad (9a)$$

$$\frac{\partial \Psi_1}{\partial \zeta} = \kappa \frac{\partial \Psi_2}{\partial \zeta} \quad \text{at } \zeta = 1, \quad (9b)$$

$$\Psi_1 = \Psi_2 \quad \text{at } \zeta = 1, \quad (9c)$$

$$\frac{\partial \Psi_2}{\partial \zeta} = 0 \quad \text{at } \zeta = N. \quad (9d)$$

From Eq. (7), the initial conditions are

$$\begin{aligned} \Psi_1(\zeta, 0) &= \theta_1^0 - \theta_1^q \\ &= C_1 \zeta + C_2, \end{aligned} \quad (10a)$$

$$\begin{aligned} \Psi_2(\zeta, 0) &= \theta_2^0 - \theta_2^q \\ &= C_3 \cosh m\zeta + C_4 \sinh m\zeta. \end{aligned} \quad (10b)$$

The constants are

$$C_1 = -m\kappa \frac{q}{B} (\sinh m - \tanh mN \cosh m), \quad (11a)$$

$$C_2 = \frac{q}{B} [m\kappa (\sinh m - \tanh mN \cosh m) - (\cosh m - \tanh mN \sinh m)], \quad (11b)$$

$$C_3 = -\frac{q}{B}, \quad (11c)$$

$$C_4 = \frac{q}{B} \tanh mN. \quad (11d)$$

Eqs. (8) are solved by separation of variables, the general solution being

$$\Psi_1 = [D_1 \cos \lambda \zeta + D_2 \sin \lambda \zeta] \exp(-\lambda^2 \tau), \quad (12a)$$

$$\Psi_2 = \left[D_3 \cos \left\{ \left(\frac{\lambda^2}{\mu} - m^2 \right)^{1/2} \zeta \right\} + D_4 \sin \left\{ \left(\frac{\lambda^2}{\mu} - m^2 \right)^{1/2} \zeta \right\} \right] \exp(-\lambda^2 \tau), \quad (12b)$$

where the D 's are constants to be determined. Substituting in the boundary conditions (9)

gives

$$\begin{pmatrix} \text{Bi} & -\lambda & 0 & 0 \\ -\lambda \sin \lambda & \lambda \cos \lambda & \kappa \beta \sin \beta & -\kappa \beta \cos \beta \\ \cos \lambda & \sin \lambda & -\cos \beta & -\sin \beta \\ 0 & 0 & -\sin \beta N & \cos \beta N \end{pmatrix} \begin{pmatrix} D_1 \\ D_2 \\ D_3 \\ D_4 \end{pmatrix} = \begin{pmatrix} 0 \\ 0 \\ 0 \\ 0 \end{pmatrix}, \quad (13)$$

where $\beta = (\lambda^2/\mu - m^2)^{1/2}$. Without loss of generality, D_2 may be assumed to be equal to unity. Then the remaining constants are obtained from

$$\begin{pmatrix} \text{Bi} & 0 & 0 \\ -\lambda \sin \lambda & \kappa\beta \sin \beta & -\kappa\beta \cos \beta \\ \cos \lambda & -\cos \beta & -\sin \beta \end{pmatrix} \begin{pmatrix} D_1 \\ D_3 \\ D_4 \end{pmatrix} = \begin{pmatrix} \lambda \\ -\lambda \cos \lambda \\ -\sin \lambda \end{pmatrix}.$$

Solving gives

$$D_1 = \frac{\lambda}{\text{Bi}}, \quad (14a)$$

$$D_3 = -\frac{\lambda}{\kappa\beta} \sin \beta \left(\cos \lambda - \frac{\lambda}{\text{Bi}} \sin \lambda \right) + \cos \beta \left(\sin \lambda + \frac{\lambda}{\text{Bi}} \cos \lambda \right), \quad (14b)$$

$$D_4 = \frac{\lambda}{\kappa\beta} \cos \beta \left(\cos \lambda - \frac{\lambda}{\text{Bi}} \sin \lambda \right) + \sin \beta \left(\sin \lambda + \frac{\lambda}{\text{Bi}} \cos \lambda \right). \quad (14c)$$

The characteristic equation obtained from Eq. (13) is

$$\begin{vmatrix} \text{Bi} & -\lambda & 0 & 0 \\ -\lambda \sin \lambda & \lambda \cos \lambda & \kappa\beta \sin \beta & -\kappa\beta \cos \beta \\ \cos \lambda & \sin \lambda & -\cos \beta & -\sin \beta \\ 0 & 0 & -\sin \beta N & \cos \beta N \end{vmatrix} = 0$$

or, after algebraic manipulations,

$$\begin{aligned} & (-\text{Bi} \lambda \cos \lambda + \lambda^2 \sin \lambda) (\cos \beta \cos \beta N + \sin \beta \sin \beta N) \\ & + (\text{Bi} \sin \lambda + \lambda \cos \lambda) (\cos \beta \sin \beta N - \sin \beta \cos \beta N) \kappa\beta = 0. \end{aligned} \quad (15)$$

The eigenvalues λ_n can be computed from this transcendental equation, and then $D_{1,n}$, $D_{3,n}$ and $D_{4,n}$ from Eq. (14) for each n . Once the eigenvalues and the constants are determined, the initial conditions (10) can be applied.

The final form of the solution of Eqs. (8) for both layers is

$$\Psi_i = \sum_{n=1}^{\infty} \frac{K_n}{I_n} \exp(-\lambda_n^2 \tau) \psi_{i,n}(\zeta), \quad (16)$$

where $i = 1, 2$, and

$$K_n = \int_0^1 \psi_{1,n}(\zeta) \Psi_1(\zeta, 0) d\zeta + \frac{\kappa}{\mu} \int_1^N \psi_{2,n}(\zeta) \Psi_2(\zeta, 0) d\zeta, \quad (17a)$$

$$I_n = \int_0^1 \psi_{1,n}^2(\zeta) d\zeta + \frac{\kappa}{\mu} \int_1^N \psi_{2,n}^2(\zeta) d\zeta, \quad (17b)$$

$$\psi_{1,n} = D_{1,n} \cos \lambda \zeta + \sin \lambda \zeta, \quad (17c)$$

$$\psi_{2,n} = D_{3,n} \cos \left\{ \left(\frac{\lambda^2}{\mu} - m^2 \right)^{1/2} \zeta \right\} + D_{4,n} \sin \left\{ \left(\frac{\lambda^2}{\mu} - m^2 \right)^{1/2} \zeta \right\}. \quad (17d)$$

Introducing Eqs. (17c) and (17d) into (17a) and (17b) gives

$$\begin{aligned} K_n &= D_{1,n} C_1 \left(\frac{\cos \lambda_n}{\lambda_n^2} + \frac{\sin \lambda_n}{\lambda_n} - \frac{1}{\lambda_n^2} \right) + D_{1,n} C_2 \left(\frac{\sin \lambda_n}{\lambda_n} \right) + C_1 \left(\frac{\sin \lambda_n}{\lambda_n^2} - \frac{\cos \lambda_n}{\lambda_n} \right) \\ &+ C_2 \left(\frac{1}{\lambda_n} - \frac{\cos \lambda_n}{\lambda_n} \right) + \frac{\kappa}{\mu} \frac{D_{3,n} C_3}{m^2 + \beta^2} \left[m \cos \beta \zeta \sinh m \zeta + \beta \sin \beta \zeta \cosh m \zeta \right]_1^N \\ &+ \frac{\kappa}{\mu} \frac{D_{3,n} C_4}{m^2 + \beta^2} \left[m \cos \beta \zeta \cosh m \zeta + \beta \sin \beta \zeta \sinh m \zeta \right]_1^N \\ &+ \frac{\kappa}{\mu} \frac{D_{4,n} C_3}{m^2 + \beta^2} \left[m \sin \beta \zeta \sinh m \zeta - \beta \cos \beta \zeta \cosh m \zeta \right]_1^N \\ &+ \frac{\kappa}{\mu} \frac{D_{4,n} C_4}{m^2 + \beta^2} \left[m \sin \beta \zeta \cosh m \zeta - \beta \cos \beta \zeta \sinh m \zeta \right]_1^N, \\ I_n &= D_{1,n}^2 \left[\frac{\zeta}{2} + \frac{1}{4\lambda_n} \sin 2\lambda_n \zeta \right]_0^1 + D_{1,n} \left[\frac{1}{\lambda_n} \sin^2 \lambda_n \zeta \right]_0^1 + \left[\frac{\zeta}{2} - \frac{1}{4\lambda_n} \sin 2\lambda_n \zeta \right]_0^1 \\ &+ \frac{\kappa}{\mu} \left\{ D_{3,n}^2 \left[\frac{\zeta}{2} + \frac{1}{4\beta_n} \sin 2\beta_n \zeta \right]_1^N + D_{3,n} D_{4,n} \left[\frac{1}{\beta_n} \sin^2 \beta_n \zeta \right]_1^N \right. \\ &\left. + D_{4,n}^2 \left[\frac{\zeta}{2} - \frac{1}{4\beta_n} \sin 2\beta_n \zeta \right]_1^N \right\}, \end{aligned}$$

where the upper and lower limits correspond to values of ζ . The C 's are in Eqs. (11), and the D 's in (14) for each value of n and λ_n . Substituting $\Psi_{1,2}$ from (16) and $\theta_{1,2}^q$ from (5) in (7) gives the transient temperature field $\theta_{1,2}(\zeta, \tau)$ which goes from an initial steady state of $\theta_{1,2}^0(\zeta)$ at $t = 0$ to another $\theta_{1,2}^q(\zeta)$ as $t \rightarrow \infty$.

5 Numerical methods

An explicit finite-volume method will be used to verify the analytical solutions as well as to extend them to a three-dimensional axisymmetric geometry. The computational domain is divided into small pieces of volume ΔV . Based on energy balance for each one of the finite volumes j , a numerical scheme is developed which enables calculation of its temperature T_j^{k+1} at time $k + 1$, given the temperature T_j^k at time k . Thus,

$$\rho C T_j^{k+1} = \rho C T_j^k + \frac{\Delta t}{\Delta V} \sum_{i=1}^n J_{j,i}^k + \Delta t \mathcal{Q}_j^k, \quad (18)$$

where $T_j^{k+1} - T_j^k$ is the increment in temperature in time step Δt , $\mathcal{Q}_j^k = Q^* + W_b C_b (T_a - T_j^k)$ is the heat generation due to metabolism as well as perfusion of blood, and $\sum J_{j,i}^k$ is the net heat inflow by conduction through the boundaries of the finite volume. The heat conduction through one boundary is approximated by

$$J_{j,i}^k = \frac{\Delta T_{j,i}^k}{R_{j,i}}, \quad (19)$$

where $\Delta T_{j,i}^k$ is the temperature difference between finite volume j and i which is the one on the other side of the boundary under consideration; $R_{j,i}$ is the thermal resistance between them.

In this explicit method, the terms on the right in Eq. (18) are calculated at the previous instant in time k for which the temperature field is known. The equation can be applied to either burned or healthy tissue by substituting the appropriate ρ and C properties. For burned tissue $\mathcal{Q}_j^k = 0$ as metabolic heat generation and blood perfusion are not present.

Numerical computations will be carried out in one-dimensional and three-dimensional axisymmetric geometries. The only difference between them is the volume ΔV in Eq. (18), the number of neighboring volumes n , and the thermal resistance $R_{j,i}$ in Eq. (19).

- *1D geometry*: The spatial coordinate is z , so that $n = 2$, $dV = dz$, and the resistance

between the volume j under consideration and its neighbor i is

$$R_{j,i} = \frac{\Delta z_i}{2k_i} + \frac{\Delta z_j}{2k_j}.$$

- *Axisymmetric geometry:* The computational domain is (r, z) , with $n = 4$. Each finite volume is a ring of $\Delta V = 2\pi r \Delta r \Delta z$. Also

$$R_{j,i} = \begin{cases} \frac{\Delta z_i}{4k_i\pi r \Delta r} + \frac{\Delta z_j}{4k_j\pi r \Delta r} & \text{for both axial neighbors,} \\ \frac{\log\{(r_i + \Delta r_i/2)/r_i\}}{2\pi k_i \Delta z_i} + \frac{\log\{r_j/(r_j - \Delta r_j/2)\}}{2\pi k_j \Delta z_j} & \text{for radially inward neighbor} \\ \frac{\log\{(r_i + \Delta r_i/2)/r\}}{2\pi k_i \Delta z_i} + \frac{\log\{r_j/(r_j - \Delta r_j/2)\}}{2\pi k_j \Delta z_j} & \text{for radially outward neighbor} \end{cases}$$

for resistances between the volume j and its neighbor i .

Special cases of heat inflows $J_{j,i}^k$ are the skin surface, where one part of the thermal resistance is convective and an external heat inflow q^* must be added. The rest of the boundaries of the computational domain have zero heat flux.

6 Results

A particular set of tissue and burn properties is used in this section. Some properties of tissue considered here are similar to those used by Weinbaum et al. [26] and Rabin and Stahovich [28]. These properties are shown in Table 1 and, unless specified otherwise, will be the ones used here for healthy tissue, and $k_1 = 0.1$ W/(m K), $\rho_1 = \rho_2$ and $C_1 = C_2$ for the burn tissue. Since reliable information about the properties of burned tissue is not available in the literature, we have arbitrarily chosen reasonable values of some of the thermophysical properties to be able to verify the correctness of the analytical solutions.

The characteristic equation (15) was solved by Newton's iterative method to determine the real eigenvalues. Table 2 presents the first 50 eigenvalues obtained for a burn of depth $H_c = 0.0025$ m and a healthy tissue substrate 19 times thicker than the burn, so that $N = 20$. The eigenvalues are positive ensuring that $\Psi_{1,2}$ from Eq. (16) both vanish as $t \rightarrow \infty$. The

number of terms of the summation was taken to be 500, and a greater number of terms did not make any difference in the results.

6.1 1D problem

To verify the analytical solution, a numerical solution of the one-dimensional problem, Eqs. (4), was obtained. The first comparison was the initial temperature distribution at $t = 0$, which is the steady-state solution of Eqs. (4), with $q = 0$. The explicit scheme given by Eq. (18) was computed repeatedly until equilibrium was reached. This solution was compared to the analytical solution given by Eqs. (5). Figure 2 shows both solutions in dimensional form; the results are very similar.

The second comparison between numerical and analytical solutions is the transient response for $t > 0$. Eq. (4) is solved numerically with the initial temperature distribution of each method obtained separately as indicated in the previous paragraph. The irradiative heat flux is taken to be $q^* = 112 \text{ W/m}^2$. Figure 3 compares the numerical and analytical transient responses for different instants in time; the dotted lines are the numerical solution at different times, and the solid lines correspond to the analytical solution described in this paper. Very good agreement between the two is evident.

6.2 Axisymmetric problem

The one-dimensional analytical solution previously obtained can be used to approximate the transient temperature field for a thin three-dimensional burned region. In the 1D approximation, at each location x, y on the skin, the tissue is assumed to be a long cylinder in the z direction. Conduction in the x - and y -directions is ignored and only that in the z -direction is included. Applying the 1D analysis at different locations gives a 3D temperature field; the x and y variations in the solution enter through the depth of the burned skin $H(x, y)$. The analysis, described in Section 4, is based on an $\epsilon \ll 1$ assumption, so that an error of $\mathcal{O}(\epsilon)$ is expected [20].

The obvious question that arises is how good the 1D analytical solution is to approximately predict an essentially 3D problem [29]. To evaluate this we solve numerically the temperature field when the burned layer is

$$H = H_c/2 \left\{ 1 + \cos \left(\pi \frac{x^2 + y^2}{R_c^2} \right) \right\}.$$

The initial temperature field is the steady-state solution, with $q^* = 0$. This is obtained using a uniform temperature T_a as initial condition, and running the axisymmetric code until equilibrium is reached. Figure 4 compares the numerical and analytical equilibrium temperature profiles at two different $r = (x^2 + y^2)^{1/2}$ positions. The surface temperature obtained by the 1D analytical approximation is slightly smaller, especially at $r = 0$, because lateral heat conduction tends to even out the temperatures in the x - and y -directions.

For $q^* = 112 \text{ W/m}^2$, Figure 5 shows a comparison of the surface temperature profile for different instant of time with initial conditions for each method obtained as described in the previous paragraph. The agreement is good, though there is a small difference. Once again, heat flow in the direction parallel to the surface of the skin, that is present in the axisymmetric numerical solution but not in the 1D analytical, has the effect of reducing the surface temperature difference of the skin at a given time. The same data are presented slightly differently in Figure 6 which shows the change in surface temperature $T_s(r, t) - T_s(r, 0)$. It can be seen that for short times both procedures give very similar responses; for longer times the difference increases, though it is still small. Difference in the calculated initial conditions causes a difference in subsequent surface temperatures, as shown in Figure 5; however, the instantaneous temperature minus the initial temperature is very small for short times, so that the temperature difference error is not as significant as is the error between the steady state analytical 1D solution and the numerical axisymmetric simulation.

6.3 Comparing the response of healthy and burned tissues

Figure 7 compares the 1D analytical, vertical temperature profiles for different instants in time in two separate cases, one with only healthy tissue and no burned layer, and the second with a 2.5 mm thick burned tissue on healthy tissue, which is a reasonable thickness in second-degree burns. It can be seen that at $t = 0$ the burned tissue is colder at the surface because (i) it does not generate metabolic heat, (ii) there is no blood perfusion in the burned tissue, and (iii) the smaller thermal conductivity of the burned region produces a larger temperature drop between the healthy substrate tissue and the external convection. At $t = 100$ s the burned tissue has reacted faster to the heat irradiation and increased its surface temperature by almost twice as much as the healthy tissue. After this initial period of very different rate of temperature increase, both the burned and unburned tissues increase the surface temperature at very similar rates, and for long times, like $t = 10000$ s, both the healthy and the burned tissues reach a new equilibrium steady state, where the heat irradiated and the heat generated within the tissue are released by convection to the surrounding air. $t = 0$ and at $t = 10000$ s represent the steady states before and after energy irradiation, and are characterized by linear temperature profiles within the burn.

6.4 Effect of burn properties

Since the properties of burned tissue are not in general known, in this part of the study the properties are varied within a range of reasonably expected values to gage their influence.

- *Thermal conductivity:* Figure 8 shows how the skin surface reacts for different thermal conductivities of the burned layer k_1 (here $k_1 = k_2/\kappa$, $k_2 = 0.2$ W/(m K), $\rho_1 = \rho_2$, $C_1 = C_2 = 4200$ J/(kg K) and $H_c = 0.0025$ m). It is seen that, at the beginning, the burned surface increases its temperature faster for smaller values of k_1 . Two factors play a role in this. For smaller thermal conductivity, the heat transfer resistance of the burn is greater, so when heat is deposited on the surface of the skin by irradiation of

the light source, it does not travel easily through the burn; energy accumulates near the surface in the form of sensible heat, causing a faster surface temperature increase. Also, because of the larger temperature difference between the initial and final states that occurs for smaller values of k_1 , the surface temperature grows faster since it has to cover a larger range.

- *Heat capacity:* Figure 9 illustrates the transient response of the burned surface as a function of the heat capacity while all other properties are constant (here $C_1 = \mu k_1 C_2 / k_2$, $\rho_1 = \rho_2$, $C_2 = 4200 \text{ J}/(\text{kg K})$, $k_1 = 0.1 \text{ W}/(\text{m K})$, $k_2 = 0.2 \text{ W}/(\text{m K})$ and $H_c = 0.0025 \text{ m}$). As expected, the tissue responds faster for smaller values of C_1 , because of larger thermal diffusivity.
- *Burn depth:* Figure 10 shows the surface temperature variation for different values of H_c (here $k_1 = 0.1 \text{ W}/(\text{m K})$, $k_2 = 0.2 \text{ W}/(\text{m K})$, $\rho_1 = \rho_2$ and $C_1 = C_2 = 4200 \text{ J}/(\text{kg K})$). The four cases of burn thickness shown in Figure 10 illustrate the quicker response of the thicker burn. The reasons for this are similar to those for Figure 8.

The variation that is observed within the range of parameters explored indicates that the transient response of the surface skin temperature is substantially affected by the parameters. This means that any thermographic method of analysis that does not simultaneously determine the actual skin properties will have inherent inaccuracies.

6.5 *Equilibrium temperature profile for different heat fluxes*

Figure 11 illustrates the final equilibrium temperature that is reached when heating the skin surface with different heat fluxes. It is clear that by increasing the heat flux applied to the surface of the skin, the surface temperature is increased in order to produce a heat convection equal to the amount of heat irradiated plus the metabolic heat generated by the skin. In all cases, the temperature profile within the burned section of the skin is linear, and the

temperature profile within the unburned part of the skin exponentially approaches the body temperature. For the set of properties used in the calculation, $q = 0.25$ (that is for $q^* = 280$ W/m²) is interesting because this heat flux makes the skin temperature uniform and equal to the body temperature, any heating above $q = 0.25$ will produce hyperthermia of the skin.

7 Discussion

Thermographs can determine the time-dependent surface temperature field $T_s(x, y, t)$ response to a step function input of incident irradiation, and from this the burn depth has to be inferred. The mathematical model and the solution described above provides a basis for that. Dickey and Holswade [17] have proposed burn depth determination based on a surface temperature variation of the form $T_s(t) = T_s(0) - \{T_s(\infty) - T_s(0)\} (1 - e^{-t/\tau})$. They approximate the time constant τ to be roughly proportional to the square of the burn depth. The present model, however, is much more realistic and takes into account many more physical factors that determine the skin temperature.

The unknown system parameters is a set of ten: $P = \{k_1, k_2, \rho_1, \rho_2, C_1, C_2, W_b, C_b, Q^*, T_a\}$ in addition to the unknown burn depth function $H(x, y)$. At a given location on the surface \bar{x}, \bar{y} , the one-dimensional analytical approximation can be used. Using surface temperature readings at 11 different instants of time gives both P and $H(\bar{x}, \bar{y})$. The same can be done at different locations \bar{x}, \bar{y} , and a regression used for P , since that should be relatively uniform over a small region.

The numerical property values used in the computations have been the best available. The method is shown to be practical since the irradiation intensity is low and the response times not too large nor too small. The flux value of 112 W/m² that was used can be obtained from a moderate intensity light bulb, and would not be injurious to a burn patient. The depth of tissue that is of interest corresponds to the thickness that may differentiate between a IIa (superficial dermal) and a IIb (deep dermal) burn. This thickness is within that of the

dermis, which is of the order of 0.3 to 3 mm. Response times are also quite moderate, and one does not need a high-speed camera nor subject the patient to hours of examination. It is possible in a few minutes to conduct a dynamic thermography test that could determine the burn thickness without *a priori* knowledge of the specific values of the material properties of the burned and unburned skin for that patient in the area of the burn.

8 Conclusions

The procedure described in this paper calculates the transient temperature response of burned skin to a step function heat flux applied at the surface. This result is important for application to burn thickness determination because the material properties there are also usually unknown. The skin transient response permits simultaneous calculation of the burn thickness and skin properties.

The mathematical model and its solution described here were tested, first by comparison with a 1D numerical solution, which proved the correctness of the analytical solution, and second with an axisymmetric numerical solution, which served to determine the validity of the 1D approximation. The parametric dependence of the thermal response of the skin surface to a superficial heat flux was analyzed showing that the two most important parameters are the thermal barrier produced by the burn (which includes the burn thickness and burn thermal conductivity) and the heat capacity of the burn, which affects the thermal diffusivity of the burn. The study also shows that simultaneous determination of system properties, that is enabled by dynamic thermography, is crucial for the accuracy of burn depth determination. To assess the practical use of the model and the solution presented here, it is necessary to proceed to experiments on skin and real or artificially simulated burns.

Acknowledgment

R.R.-M. thanks CONACyT (México) for support to projects FMSLP-C01-2007-62604 and CB-2008-84618. F.J.G. acknowledges CONACyT for support through FMSLP-2005-C01-28, CB-2006-60349 and FMSLP-C01-87127. M.S. thanks NSF for Award No. 0849549.

References

- [1] R.P. Clark and M.R. Goff. Medical thermography—Current status. *Proceedings of SPIE*, 1320:242–250, 1990.
- [2] D. Park, N.H. Seung, J. Kim, H. Jeong, and S. Lee. Infrared thermography in the diagnosis of unilateral carpal tunnel syndrome. *Muscle and Nerve*, 36(4):575–576, 2007.
- [3] F.M.M. Ya'ish, J.P. Cooper, and M.A.C. Craigen. Thermometric diagnosis of peripheral nerve injuries—Assessment of the diagnostic accuracy of a new practical technique. *Journal of Bone and Joint Surgery*, 89B(7):933–939, 2007.
- [4] L. Weibel, M.C. Sampaio, M. T. Visentin, K.J. Howell, P. Woo, and J.I. Harper. Evaluation of methotrexate and corticosteroids for the treatment of localized scleroderma (morphoea) in children. *British Journal of Dermatology*, 155(5):1013–1020, 2006.
- [5] V. Shusterman, K.P. Anderson, and O. Barnea. Spontaneous skin temperature oscillations in normal human subjects. *American Journal of Physiology-Regulatory Integrative and Comparative Physiology*, 273(3):R1173–R1181, 1997.
- [6] J.F. Head and R.L. Elliott. Infrared imaging: Making progress in fulfilling its medical promise. *IEEE Engineering in Medicine and Biology Magazine*, 21(6):80–85, 2002.
- [7] B.F. Jones. A reappraisal of the use of infrared thermal image analysis in medicine. *IEEE Transactions on Medical Imaging*, 17(6):1019–1027, 1998.
- [8] J.P. Gore and L.X. Xu. Thermal imaging for biological and medical diagnostics. In T. Vo-Dinh, editor, *Biomedical Photonics Handbook*, Chap. 17. CRC Press, 2003.
- [9] J.S. Teich. Digital infrared imaging for medicine. Recent advances in I.R. focal plane

- array imaging technology. In *Engineering in Medicine and Biology Society, 1996. Proceedings of the 18th Annual International Conference of the IEEE*, 31 Oct.-3 Nov. 1996, pages 2079–2080, 1996.
- [10] T.L. Williams. *Thermal Imaging Cameras: Characteristics and Performance*. CRC Press, Boca Raton, FL, 2009.
- [11] P.G. Shakespeare. Looking at burn wounds: The A.B. Wallace Memorial Lecture. *Burns*, 18(4):287–295, 1991.
- [12] J. Ruminski, M. Kaczmarek, A. Renkielska, and A. Nowakowski. Thermal parametric imaging in the evaluation of skin burn depth. *IEEE Transactions on Biomedical Engineering*, 54(2):303–312, 2007.
- [13] D.J. McGill, K. Sørensen, I.R. MacKay, I. Taggart, and S.B. Watson. Assessment of burn depth: A prospective, blinded comparison of laser doppler imaging and videomicroscopy. *Burns*, 33(7):833–842, 2007.
- [14] W.-P. Zhu and X.-R. Xin. Study on the distribution pattern of skin temperature in normal Chinese and detection of the depth of early burn wound by infrared thermography. *Annals of the New York Academy of Sciences*, 888:300–313, 1999.
- [15] A. Renkielska, A. Nowakowski, M. Kaczmarek, M.K. Dobke, J. Grudziński, A. Karmolinski, and W. Stojek. Static thermography revisited—An adjunct method for determining the depth of the burn injury. *Burns*, 31:768–775, 2005.
- [16] G.G. Gardner and C.J. Martin. The mathematical modelling of thermal responses of normal subjects and burned patients. *Physiological Measurements*, 15:381–400, 1994.
- [17] F.M. Dickey and S.C. Holswade. Method and apparatus to measure the depth of skin burns, U.S. Patent 6381488, April 30, 2002.
- [18] A.R. Moritz and F.C. Henriques. Studies of thermal injury: II. The relative importance of time and surface temperature. *American Journal of Pathology*, 23:695–720, 1947.
- [19] E.Y.-K. Ng and L.T. Chua. Prediction of skin burn injury. Part 1: Numerical modelling.

- Part 2: Parametric and sensitivity analysis. *Proceedings of the Institution of Mechanical Engineers Part H—Journal of Engineering in Medicine*, 216(3):157–170, 171–183, 2002.
- [20] R. Romero-Méndez, J.N. Jiménez-Lozano, M. Sen, and F.J. González. Analytical solution of the Pennes equation for burn depth determination from infrared thermographs. *Mathematical Medicine and Biology*, 2009. In press.
- [21] H.H. Pennes. Analysis of tissue and arterial blood temperatures in the resting human forearm. *Journal of Applied Physiology*, 1(2):93–122, 1948.
- [22] C.K. Charny. Mathematical models of bioheat transfer. *Advances in Heat Transfer*, 22:19–155, 1992.
- [23] H. Arkin, L.X. Xu, and K.R. Holmes. Recent developments in modeling heat-transfer in blood-perfused tissues. *IEEE Transactions on Biomedical Engineering*, 41(2):97–107, 1994.
- [24] K.R. Diller, J.W. Valvano, and J.A. Pearce. Bioheat transfer. In F. Kreith, editor, *The CRC Handbook of Thermal Engineering*. Section 4.4, pages 114–187. CRC Press, Boca Raton FL, 2000.
- [25] M.M. Chen and K.R. Holmes. Microvascular contributions in tissue heat transfer. *Annals of the New York Academy of Sciences*, 335:137–150, 1980.
- [26] S. Weinbaum, L.M. Jiji, and D.E. Lemons. Theory and experiment for the effect of vascular microstructure on surface tissue heat-transfer. Part 1. Anatomical foundation and model conceptualization. Part 2. Model formulation and solution. *ASME Journal of Biomechanical Engineering*, 106(4):321–330 and 331–340, 1984.
- [27] A.R.A. Khaled and K. Vafai. The role of porous media in modeling flow and heat transfer in biological tissues. *International Journal of Heat and Mass Transfer*, 46(26):4989–5003, 2003.
- [28] Y. Rabin and T.F. Stahovich. Cryoheater as a means of cryosurgery control. *Physics in Medicine and Biology*, 48(5):619–632, 2003.

- [29] E.Y.-K. Ng and L.T. Chua. Comparison of one- and two-dimensional programmes for predicting the state of skin burns. *Burns*, 28(1):27–34, 2002.
- [30] J. Liu, X. Chen, and X. Xu. New thermal wave aspects on burn evaluation of skin subjected to instantaneous heating. *IEEE Transactions on Biomedical Engineering*, 46(4):420–428, 1999.

Table 1: Properties of homogeneous, well-irrigated tissue [30], [28] and convective conditions.

Property	value	units
C_b	4200	J/(kg K)
k	0.2	W/(m K)
W_b	0.5	kg/m ³ s
Q^*	200	W/m ³
h	10	W/m ² K
T_a	36.5	°C
T_∞	22.5	°C
H	0.0025	m

Table 2: First 50 eigenvalues λ_n from Eq. (15).

n	0	10	20	30	40
+1	0.000000	1.991050	4.165542	6.323892	8.485396
+2	0.367119	2.201492	4.380001	6.545524	8.702900
+3	0.435624	2.415062	4.592247	6.766618	8.922404
+4	0.582216	2.631381	4.803242	6.986580	9.143308
+5	0.765202	2.849762	5.014607	7.204793	9.365007
+6	0.962951	3.069482	5.227801	7.420737	9.586931
+7	1.166510	3.289872	5.443466	7.634277	9.808525
+8	1.371854	3.510303	5.661468	7.846053	10.029211
+9	1.577420	3.730154	5.881283	8.057521	10.248379
+10	1.783407	3.948777	6.102290	8.270309	10.465448

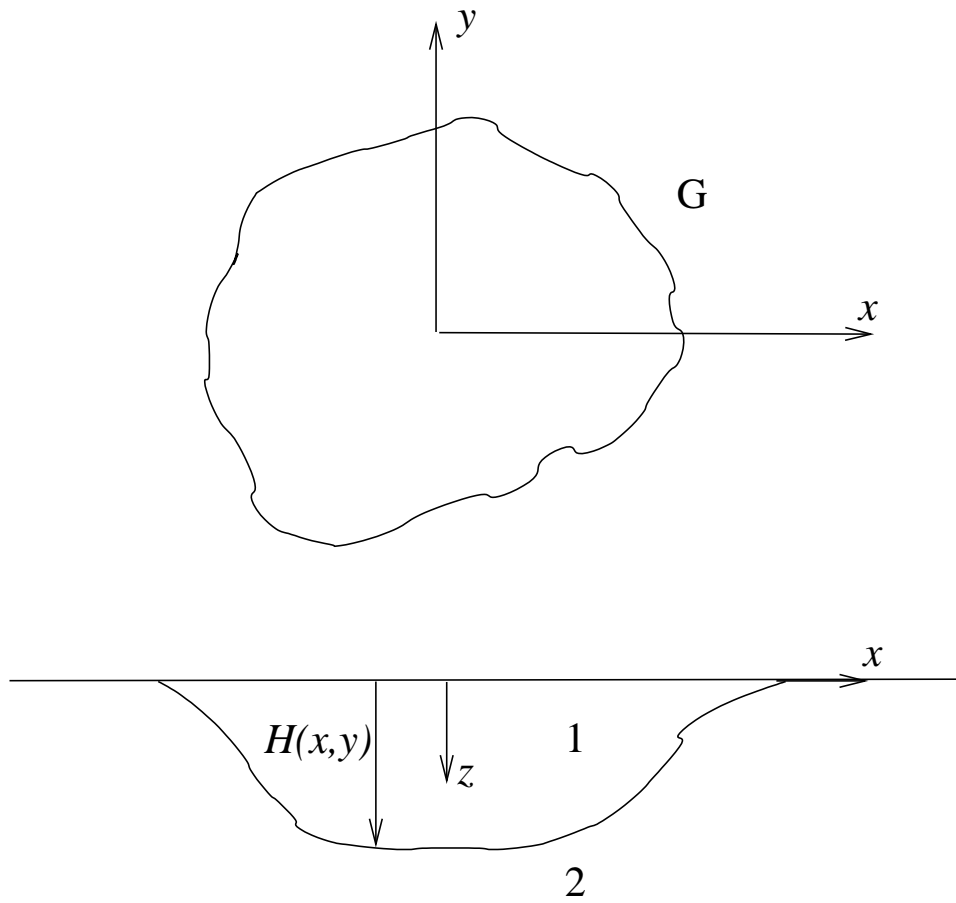


Figure 1: Geometry of burned tissue.

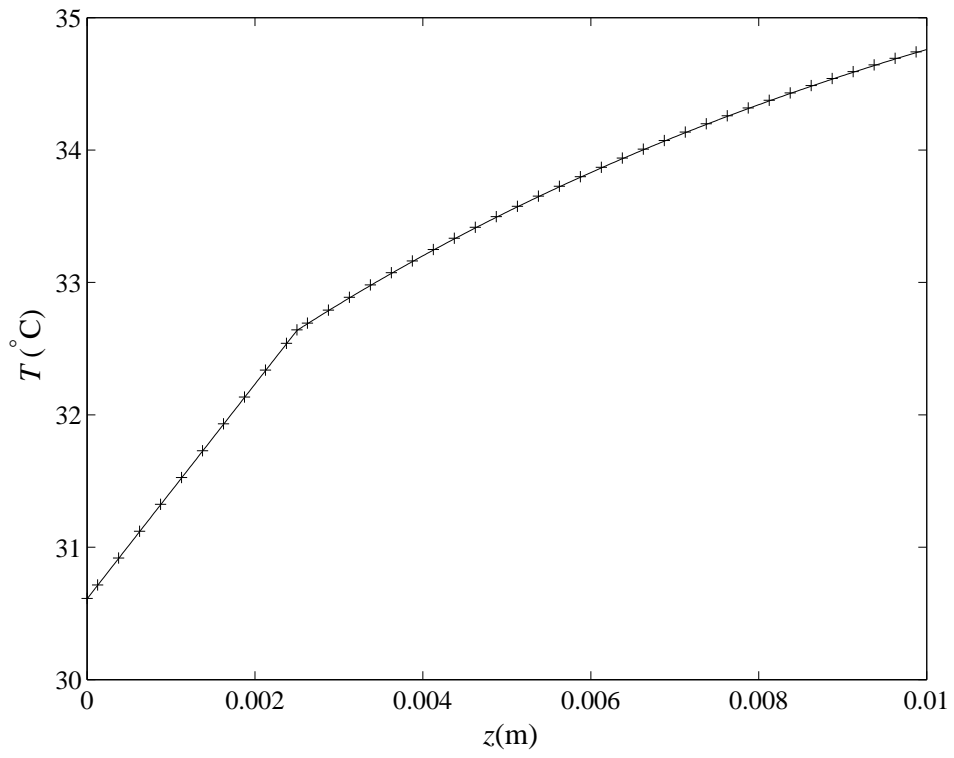


Figure 2: Vertical profile of initial temperature in one-dimensional burn; solid line analytical, + numerical.

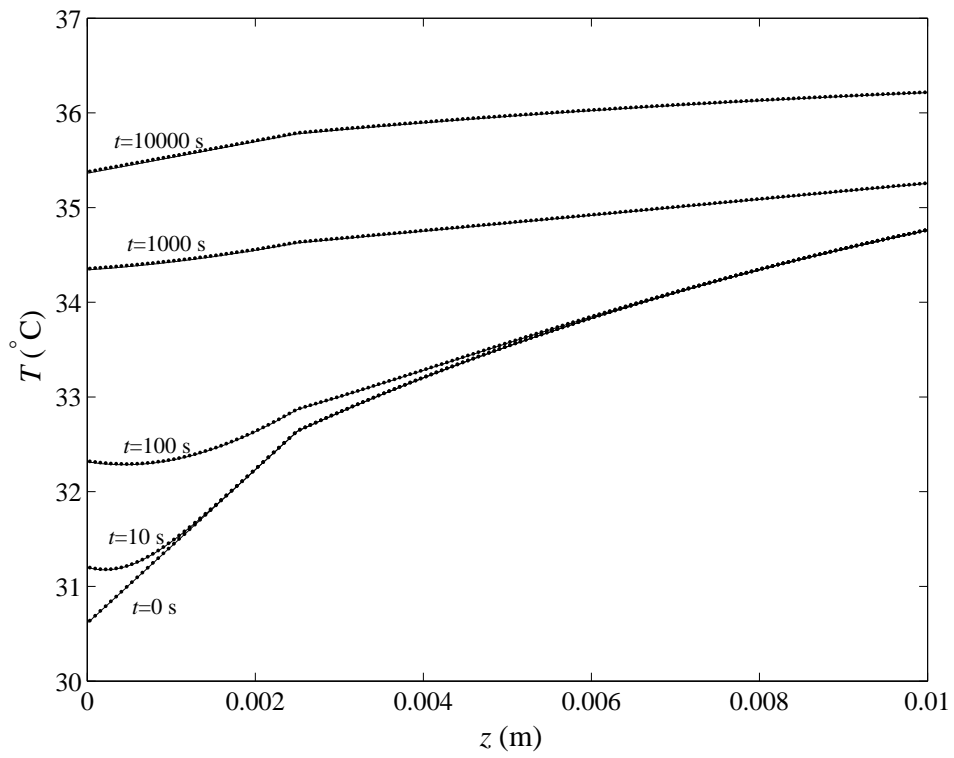


Figure 3: Vertical profile of temperature at different times; solid lines analytical, dots numerical.

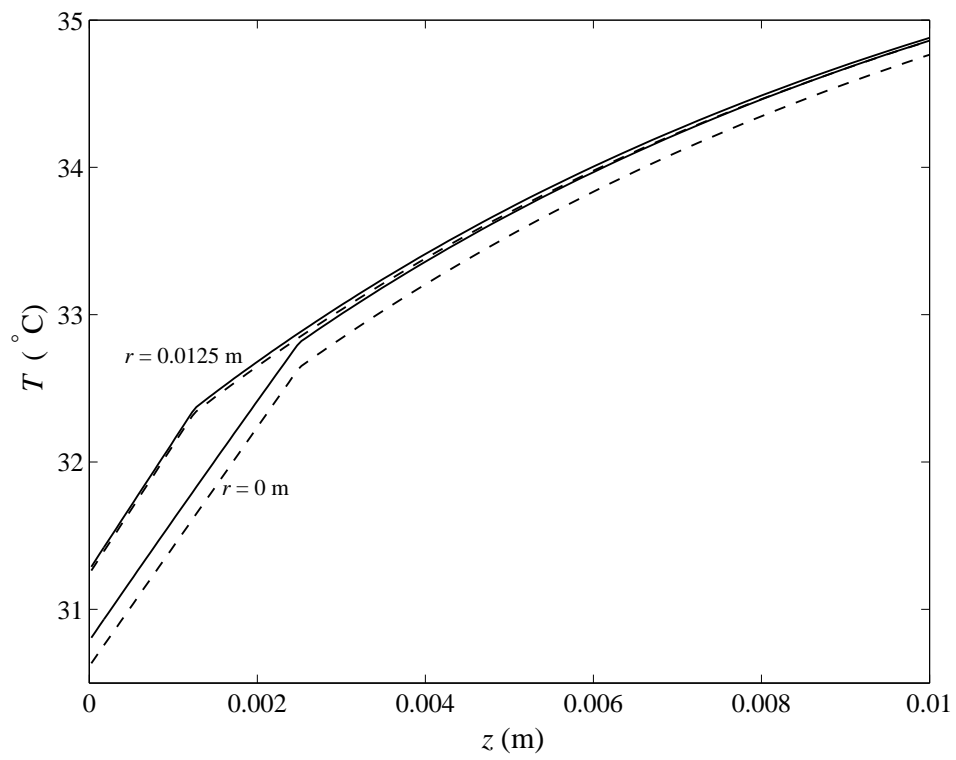


Figure 4: Steady-state vertical temperature profile $T(r, z)$ for axisymmetric burn; solid lines 3D numerical, dashed lines 1D analytical.

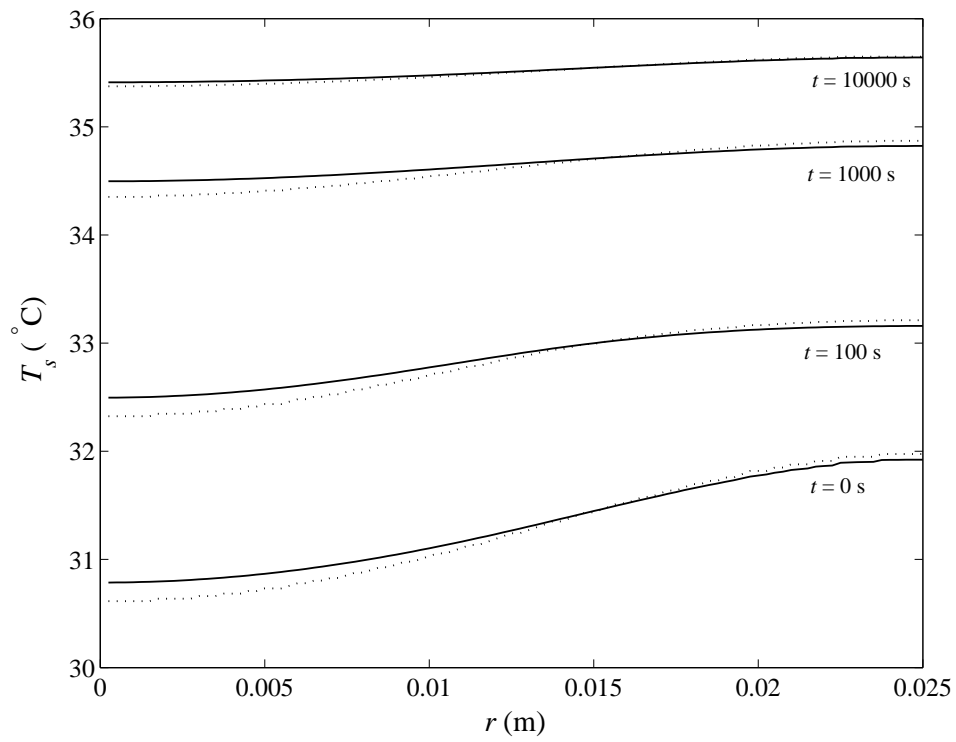


Figure 5: Surface temperature profile $T_s(r, t)$ for axisymmetric burn; solid lines numerical, dotted lines analytical.

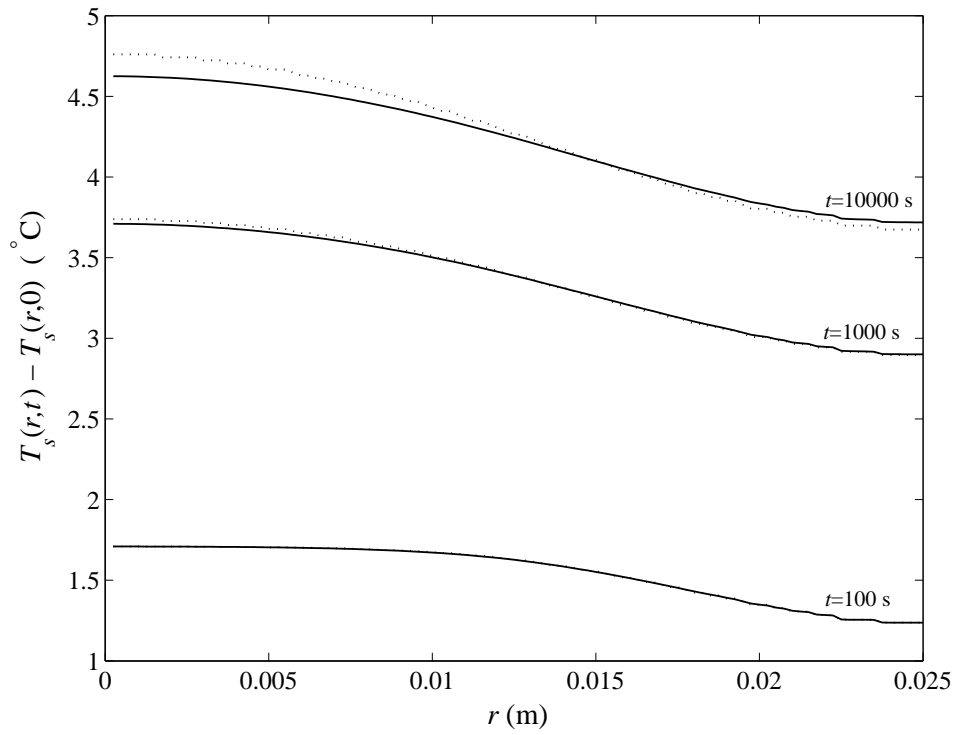


Figure 6: Surface temperature increase $T_s(r, t) - T_s(r, 0)$ for axisymmetric burn; solid lines numerical, dotted lines analytical.

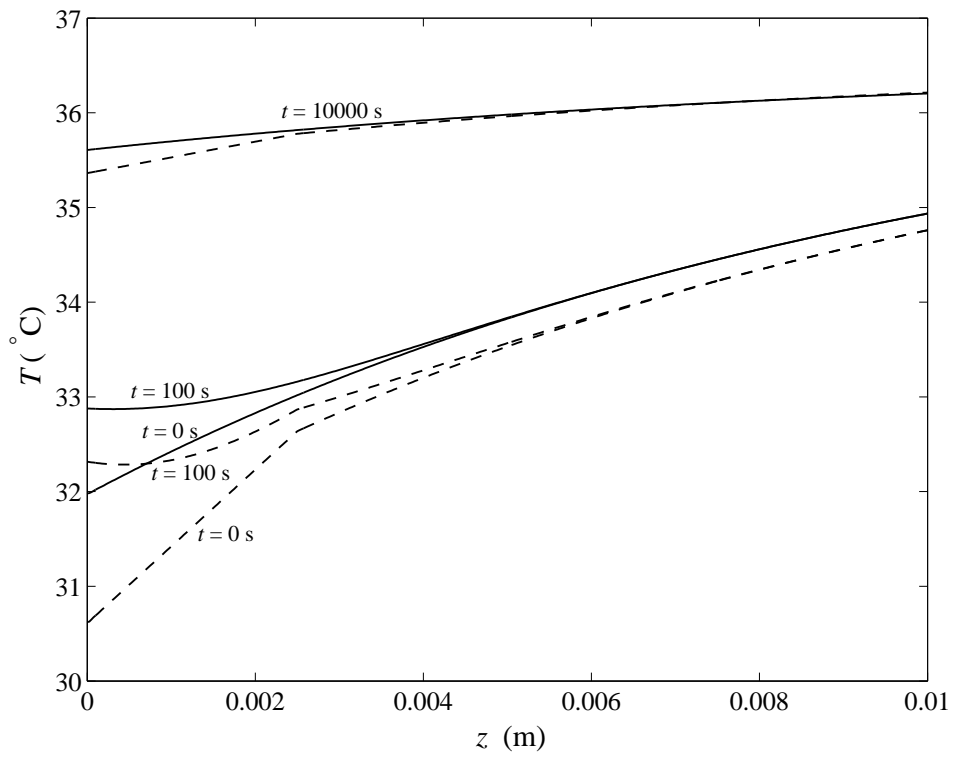


Figure 7: Transient vertical temperature profile $T(z, t)$ in one-dimensional burn; solid lines healthy tissue only, -- burned tissue with $H = 2.5$ mm.

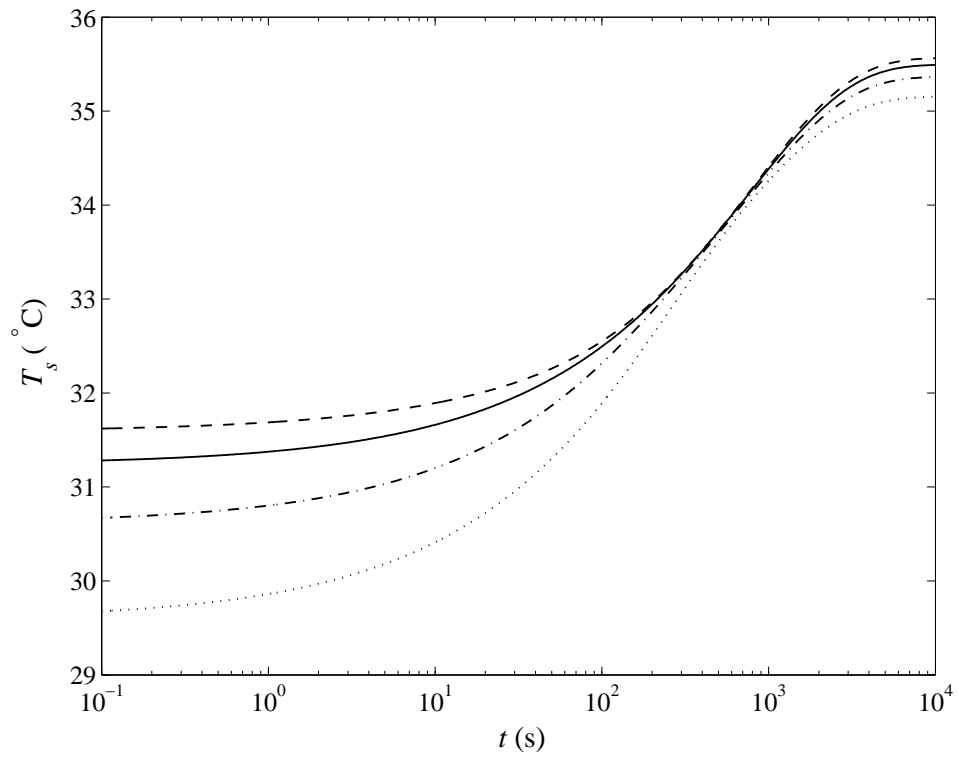


Figure 8: Transient surface temperature $T_s(t)$ in one-dimensional burn for different burn thermal conductivity ratios. $-- \kappa = 0.5$, $— \kappa = 1$, $- \cdot - \kappa = 2$, $\cdot \cdot \cdot \kappa = 4$.

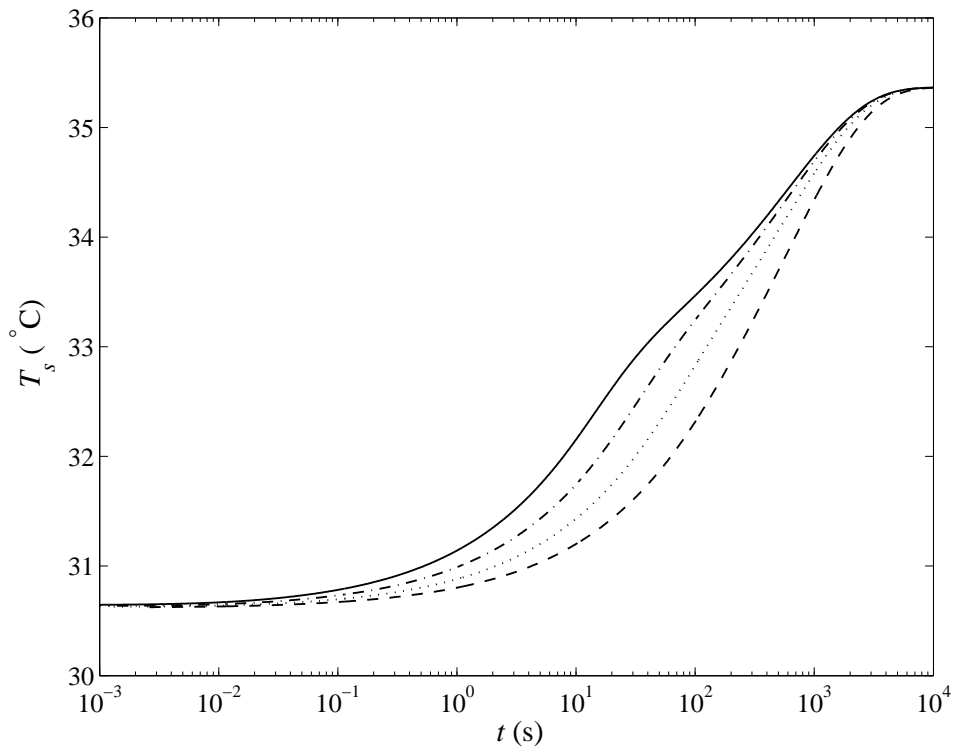


Figure 9: Transient surface temperature $T_s(t)$ in one-dimensional burn for different thermal diffusivity ratios. — $\mu = 0.25$, - · - $\mu = 0.5$, · · · $\mu = 1$, - - $\mu = 2$.

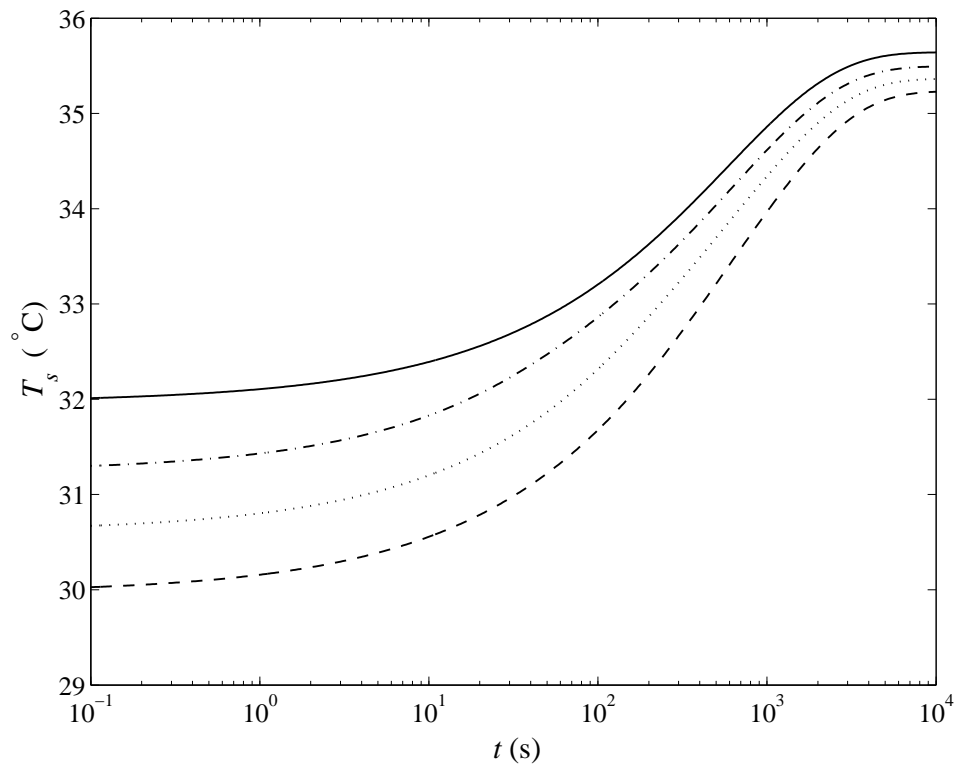


Figure 10: Transient surface temperature $T_s(t)$ in one-dimensional burn for different burn depths. — $H_c = 0.25$ mm, - · - $H_c = 1.25$ mm, · · · $H_c = 2.5$ mm, -- $H_c = 4$ mm.

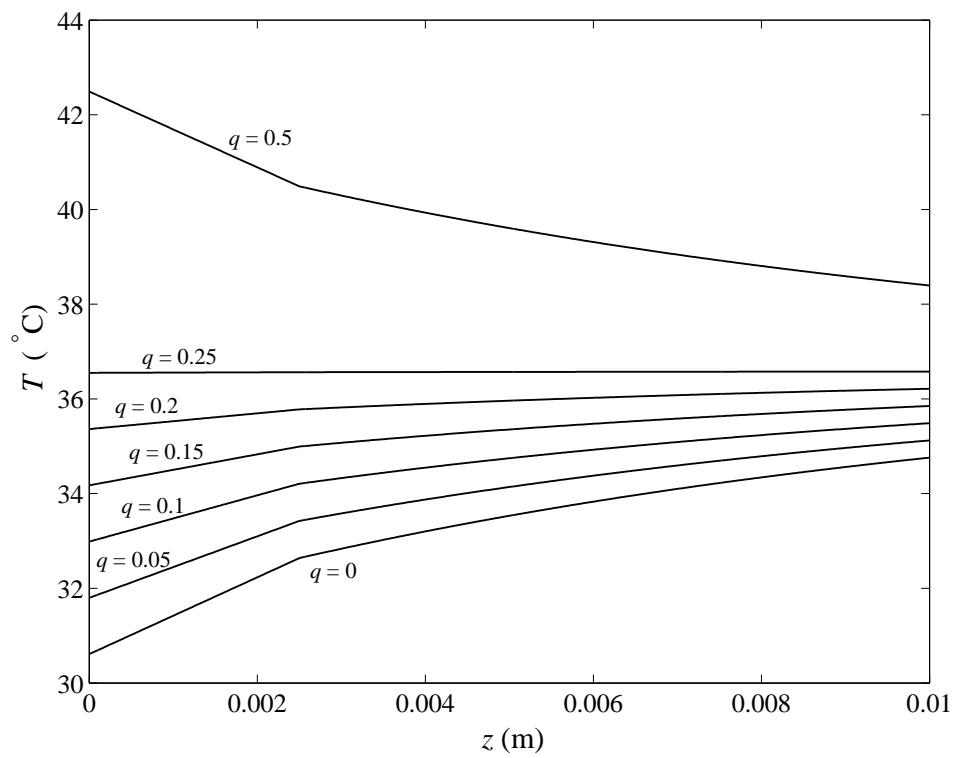


Figure 11: Final steady-state vertical temperature profile in one-dimensional burn $T(z)$ for different heat flux q .